Nonlinear Relaxation Behavior of Diblock Copolymer Micellar Dispersions: Effects of Corona−Matrix and Corona−Corona Entanglements

Yumi Matsumiya and Hiroshi Watanabe*

Institute for Chemical Research, Kyoto University, Uji, Kyoto 611-0011, Japan

Received July 16, 2004; Revised Manuscript Received October 5, 2004

ABSTRACT: The nonlinear relaxation modulus was examined for styrene−isoprene (SI) diblock copolymer micelles having rigid (glassy) S cores and flexible I corona blocks. These micelles, being dispersed randomly in entangling and/or nonentangling matrices of homopolyisoprene (hI), exhibited fast and slow relaxation processes. The fast process reflected the orientational relaxation of the corona I blocks, and the slow process detected the relaxation of the Brownian stress σ_B. This σ_B reflected the anisotropy of micelle distribution and relaxed through the micelle diffusion. The fast and slow processes exhibited the nonlinear damping of the modulus under large step strains (γ), and the time-strain separability was observed for both processes in either the entangling or nonentangling matrices. For the fast process, the damping function $h_f(\gamma)$ hardly changed with the SI micelle concentration C_{SI} and matrix molecular weight M_{matrix} and was close, in magnitude, to $h(\gamma)$ of homopolymers. The nonlinearity of the corona relaxation characterized with this $h_f(\gamma)$ was attributed to retraction of the strain-elongated corona blocks occurring prior to their rotational motion (orientational relaxation). The damping function $h_s(\gamma)$ of the slow process, being smaller than $h_f(\gamma)$, decreased with increasing C_{SI}. This nonlinearity of the slow process, similar to that of Brownian suspensions, reflected the γ-insensitivity of the micelle distribution anisotropy for large γ, and the strong C_{SI} dependence of $h_s(\gamma)$ was attributed to relative rotation of concentrated micelles colliding with each other under large strains. (This rotation is similar to random mixing, thereby reducing the anisotropy and enhancing the damping.) Interestingly, the damping of the slow process was weaker in the entangling matrices than in the nonentangling matrices. This effect of the corona−matrix entanglement, observed for both the concentrated and dilute micelles with and without corona−corona entanglement, was attributed to the elasticity of the entangling matrices that disturbed the relative rotation of the mutually colliding micelles. A similar elastic effect of the corona−corona entanglement on the damping behavior was also noted.

1. Introduction

Styrene−isoprene (SI) diblock copolymers with relatively small S content form spherical micelles having S cores and I corona in homopolyisoprene (hI) matrices. These micelles are randomly dispersed in the matrix when the intercorona osmotic interaction is efficiently screened by the matrix hI chains, i.e., when the micelles are not highly concentrated and the matrix chains are sufficiently shorter than the corona blocks.[1−3] Such micellar dispersions behave as viscoelastic liquids to exhibit multistep relaxation:[1−9] After the relaxation of the matrix chains, the micelles exhibit fast and slow relaxation processes. The fast process represents the orientational relaxation of the corona I blocks, and the slow process detects the relaxation of the Brownian stress σ_B due to micelle diffusion.[6−9] This σ_B is equivalent to the viscoelastic stress of Brownian suspensions of nanoparticles[10−16] and reflects an anisotropy of the spatial distribution of the micelles raised by the applied strain.

Under large strain/fast flow, the micellar dispersions exhibit significant nonlinearities according to the above relaxation mechanisms. Previous studies[6,17] revealed that the SI micelles having no corona−corona entanglement and being dispersed in a nonentangling matrix exhibit nonlinear damping of the relaxation modulus $G(t,\gamma)$ for both the fast and slow processes. The time-strain separability held for each process[17] and the non-Newtonian behavior under fast flow were well correlated with this damping behavior through a BKZ constitutive equation.[18] The nonlinearity of the fast process (corona relaxation), characterized with a damping function $h_f(\gamma)$ that was hardly dependent on the micelle concentration and close to $h(\gamma)$ of homopolymers, was attributed to retraction of the strain-elongated corona blocks occurring faster than their rotational motion (orientational relaxation). In contrast, the damping was larger for the slow process, and its damping function $h_s(\gamma)$ decreased strongly with increasing micelle concentration. These features of the slow process were very similar to those of the Brownian suspensions[15,16] and reflected the nature of the Brownian stress σ_B:[17] The distribution anisotropy of the micelles becomes insensitive to the applied strain γ with increasing γ. Thus, for large γ, σ_B determined by this anisotropy is only weakly dependent on γ to give the strong damping of $G(t,\gamma)$ ($= \sigma_B/\gamma$ at long times t). This damping is enhanced when the strain leads to intermicellar collision, thereby activating relative rotation of the colliding micelles and reducing the distribution anisotropy, as similar to the situation for the Brownian suspensions of silica particles.[15,16] The strong decrease of $h_s(\gamma)$ with the micelle concentration is attributable to this collision-induced reduction of the anisotropy.

Thus, experiments have revealed the similarities in the nonlinear behavior of the micelles having no corona−corona and corona−matrix entanglements and the Brownian silica suspensions. For the micelles having

* To whom all correspondence should be addressed.

10.1021/ma048544z CCC: $27.50
Published on Web 11/18/2004

Table 1. Characteristics of Samples

sample code	$10^{-3}M_S$	$10^{-3}M_I$	M_w/M_n
SI Diblock Copolymer			
SI 68-122[a]	67.8	122.0	1.06
SI 14-29[b]	13.9	28.8	1.06
Homopolyisoprene			
I-33[c]		33.4	1.04
I-19[c]		19.2	1.05
I-8[c]		8.2	1.03
I-2[d]		1.6	1.14

[a] M_S (weight-average molecular weight) of the precursor S block was determined from GPC elution volume calibration with monodispese polystyrenes (Tosoh), and M_I was evaluated from this M_S value and the UV/RI GPC signal ratio measured for the copolymer sample. The M_w/M_n ratio of the copolymer sample was evaluated from the elution volume calibration. [b] Synthesized and characterized in the previous study.[2] [c] M_I (weight-average molecular weight) and M_w/M_n ratio were determined from GPC elution volume calibration with standard monodispese homopolyisoprenes. [d] M_n of I-2 was determined from a ratio of ^{1}H NMR signals from the *sec*-butyl group (initiator fragment) and monomers, and M_w/M_n ratio was evaluated with the GPC elution volume calibration. The M_I shown in Table 1 (= weight-average molecular weight) was obtained from these M_n and M_w/M_n values.

these entanglements, the linear viscoelastic behavior was studied,[2,3,5] but no experiment was made in the nonlinear regime. Thus, we examined effects of the entanglements on the nonlinear relaxation of the SI micelles. It turned out that the corona−matrix entanglement weakened the nonlinearity possibly because the elasticity of entangling matrices disturbed the relative rotation of colliding micelles. A similar elastic effect of the corona−corona entanglement on the damping behavior was also noted. Details of these effects are presented in this paper.

2. Experimental Section

2.1. Materials. A styrene−isoprene diblock copolymer, SI 68-122, and four homopolyisoprene (hI) samples, I-33, I-19, I-8, and I-2, were anionically synthesized with *sec*-butyllithium in benzene. These samples were characterized with GPC (CO-8020 and DP-8020, Tosoh) equipped with refractive index (RI) and ultraviolet absorption (UV) monitors (LS-8000 and UV-8020, Tosoh). The I-2 sample was also characterized with ^{1}H NMR (JNM-AL400, JEOL). The molecular characteristics of these samples are summarized in Table 1, where the code numbers indicate the molecular weights in unit of 1000.

The systems subjected to rheological measurements were 5 and 15 wt % blends of SI 68-122 in the hI samples and a 15 wt % blend of a previously utilized SI copolymer,[17,18] SI 14-29 (molecular characteristics shown in Table 1), in I-19. These blends were prepared by first dissolving prescribed masses of the SI and hI samples in benzene to make homogeneous solutions (of concentration ≅5 wt %) and then allowing benzene to thoroughly evaporate. Since the S content in these blends was small (<6 vol %), spherical micelles having S cores and I corona were formed in these blends. The matrix hI chains were considerably shorter than the corona I blocks and efficiently screened the intercorona osmotic interaction. Thus, the SI micelles were randomly dispersed in the hI matrices to exhibit the terminal relaxation reflecting their diffusion. (The corona I blocks of these micelles should have been in the wet brush state.[9])

The corona I blocks of the SI 68-122 and 14-29 micelles and the I-33 and I-19 matrix chains have the molecular weights well above the entanglement molecular weight for bulk hI,[19] $M_e° = 5 \times 10^3$. Thus, the corona−matrix entanglement was well developed in all SI/I-33 and SI/I-19 blends examined. The corona blocks are barely entangled with the matrix chains in the SI/I-8 blends ($M_{matrix} = 1.6M_e°$), and no corona−matrix entanglement was formed in the SI/I-2 blends ($M_{matrix} = 0.3M_e°$). Furthermore, the neighboring micelles in the 15 wt % SI 68-122 blends were mutually entangled through their corona I blocks, as judged from the corona molecular weight ($M_I = 122 \times 10^3$) being larger than a critical molecular weight for the corona−corona entanglement, $M_e = M_e°/\phi_{ccorona} = 50 \times 10^3$ (ϕ_{corona} = corona volume fraction in the matrix phase). On the other hand, the micelles were not mutually entangled in the 5 wt % SI 68-122 blends and 15 wt % SI 14-29 blend.

Hereafter, the micelles with and without mutual entanglements are simply referred to as the *concentrated* and *dilute* micelles, respectively, although the dilute micelles examined here are not in the infinitely dilute state.

2.2. Measurements. For the SI/hI micellar dispersions (blends), rheological measurements were conducted with a laboratory rheometer (ARES, Rheometrics) in a cone−plate geometry of the plate diameter = 2.5 cm and the gap angle between cone and plate = 0.1 rad.

Dynamic measurements were conducted at several temperatures (−20 °C ≤ T ≤ 80 °C) below T_g of the S block (micelle core) but well above T_g of the corona I blocks and hI matrix chains. The amplitude of the oscillatory strain was kept small (≤0.05) to ensure the linearity of the storage and loss moduli, $G'(\omega)$ and $G''(\omega)$, measured as functions of the angular frequency ω. The time−temperature superposition was valid for these G' and G'' data (because the micelle structure did not change with T at $T < T_g^{PS}$), and the data were reduced at 25 °C.

For all SI/hI blends, stress relaxation experiments against step strains of magnitude γ (≤4) were conducted at $T = 5$ and 25 °C to measure the nonlinear relaxation modulus $G(t,\gamma)$ as a function of time t. The $G(t,\gamma)$ data at 5 °C were reduced at 25 °C with the aid of the shift factor for the linear viscoelastic G' and G'' data. For the series of the SI/I-19 blends, steady flow measurements were also conducted at 25 °C for completeness of rheological characterization.

3. Results and Discussion

3.1. Overview of Linear Viscoelastic Behavior. For the SI 68-122/I-19 blends with the SI concentration C_{SI} = 5 and 15 wt %, Figure 1 shows the storage and loss moduli G' and G'' reduced at 25 °C. Spherical SI micelles with glassy S cores and flexible I corona are formed in these blends. As explained earlier, the corona blocks are entangled with the matrix I-19 chains in both blends, and the neighboring micelles in the 15 wt % blend are mutually entangled through their corona. The dotted curves indicate the behavior of the matrix I-19 chains in their bulk state. The blends clearly exhibit three-step relaxation process, with the highest-ω process being attributed to the orientational relaxation of the matrix chains. The middle-ω and low-ω processes detect the fast and slow relaxation processes of the SI micelles. Similar behavior was observed for all SI/hI blends examined.

Diffusion experiments[7−9] and analysis of the terminal relaxation time[2,3,6] indicated that the slow process of similar SI micelles detects the relaxation of the Brownian stress σ_B due to the micelle diffusion over a distance ≅ the S core diameter. Dielectric experiments[2,6,8] (detecting the motion of the corona I blocks having electrical dipoles parallel along the chain backbone) and analysis of the viscoelastic mode distribution[2,6,7] indicated that the fast process of the micelles is assigned to the orientational relaxation of individual I blocks. This assignment was confirmed also for our SI micelles, as explained below.

For star-branched homopolymers having less than 18 arms per chain, the complex modulus normalized with the arm molecular weight M_{arm} and concentration C, $G_r^* = M_{arm}G^*/C$ with $G^* = G' + iG''$, is universally dependent on the normalized frequency $\omega\tau_{star}$ at low ω

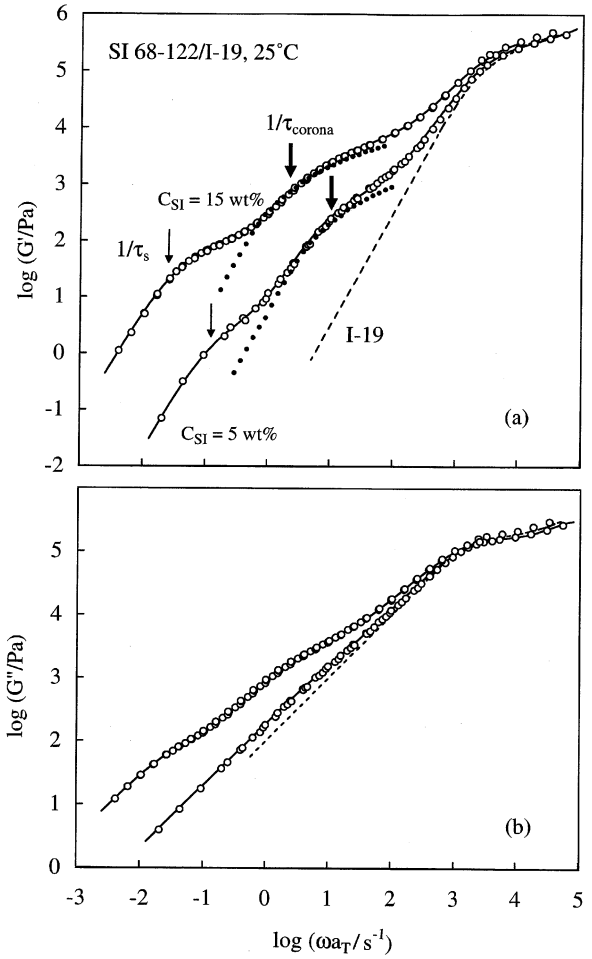

Figure 1. Linear viscoelastic behavior of the 5 and 15 wt % SI 68-122/I-19 micellar blends at 25 °C (unfilled circles). The dotted curves denote the behavior of the matrix I-19, and the small filled circles show the behavior of the corona I blocks deduced from that of star hI solutions. Thick and thin arrows indicate the relaxation frequencies of the fast and slow processes, $1/\tau_{corona}$ and $1/\tau_s$. For further details, see text.

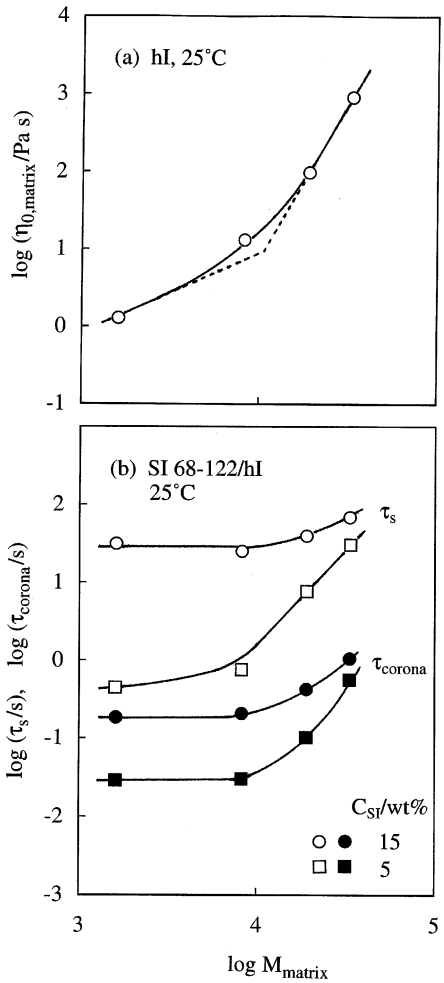

Figure 2. Dependence of (a) zero-shear viscosity of the matrix hI and (b) relaxation times of the fast and slow processes of 15 and 5 wt % SI 68-122/hI blends at 25 °C on the matrix molecular weight. WLF correction was made for the data in the shortest I-2 matrix to reduce the data at an isofrictional state (= 25 °C in higher-M matrices).

(τ_{star} = relaxation time of the star arms).[20] Considering this universality, we utilized G^* data of star hI in the literature[21] to estimate G_{star}^* of star solutions having M_{arm} and C identical to M_I and C_I of the micellar corona I blocks. Since the corona relaxation in the I-19 matrix is affected by the steric hindrance from the glassy S core[2−5] as well as the corona−matrix entanglement,[5] the estimated G_{star}^* (being free from these effects) did not agree with the G^* data of our SI/I-19 blends when plotted against uncorrected ω. However, this G_{star}^* agreed well with the blend data when plotted against an appropriately shifted frequency $\lambda\omega$; see G_{star}' shown with the filled circles in Figure 1. This agreement means that the relaxation mode distribution of fast process of our SI micelle is close to that of the star arms, confirming that this process is attributed to the orientational relaxation of individual corona I blocks.

3.2. Linear Viscoelastic Relaxation Times. The above agreement between G^* of the SI/hI blends and star solutions allowed us to evaluate the corona relaxation time τ_{corona} from the known shift factor λ and the relaxation time of the star arm τ_{star} as $\tau_{corona} = \tau_{star}/\lambda$. This τ_{corona} well specifies the terminal regime of the fast process; see thick arrows in Figure 1.

Similarly, the zero-shear viscosity and steady-state compliance due only to the corona relaxation were evaluated as $\eta_{0,corona} = \eta_{0,star}/\lambda$ and $J_{corona} = J_{star}$, with $\eta_{0,star}$ and J_{star} being the know viscosity and compliance of the star solution. From these $\eta_{0,corona}$ and J_{corona} values together with the viscosity and compliance data of the SI/hI blends and pure matrix (obtained from their G^* data), we evaluated the terminal relaxation time of the slow process as[7]

$$\tau_s = \frac{J_{blend}\eta_{0,blend}^2 - J_{corona}\eta_{0,corona}^2 - \phi_{matrix}J_{matrix}\eta_{0,matrix}^2}{\eta_{0,blend} - \eta_{0,corona} - \phi_{matrix}\eta_{0,matrix}} \quad (1)$$

Here, ϕ_{matrix} is the matrix volume fraction in the blends. This τ_s well specifies the terminal regime of the slow process; see thin arrows in Figure 1.

In Figure 2a,b, the matrix viscosity and the relaxation times of the fast/slow processes of the SI 68-122/hI blends at 25 °C are plotted against the matrix molecular weight M_{matrix}. For the lowest-M I-2 matrix having a lower T_g compared to that of the other matrices, we made a standard WLF analysis[19] to make a free-volume correction for the monomeric friction ζ. The viscosity data in this iso-ζ state show the well-known behavior[19] $\eta_{0,matrix} \propto M_{matrix}$ for $M_{matrix} < M_c$ and $\eta_{0,matrix} \propto M_{matrix}^{3.5}$

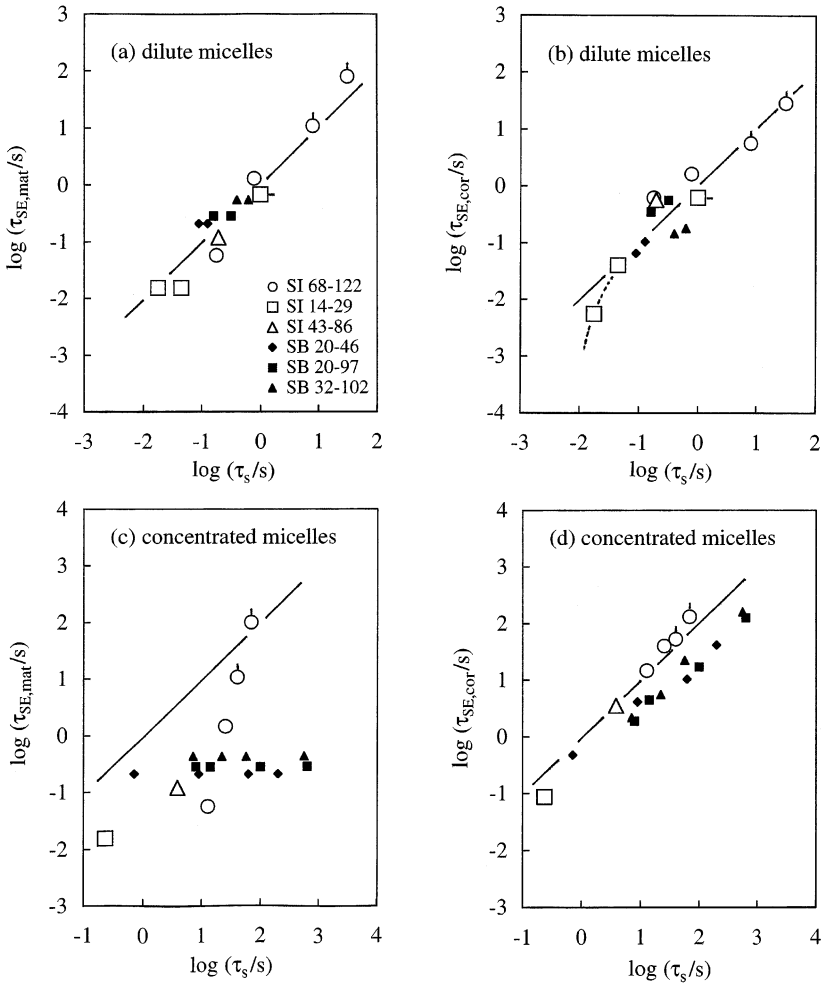

Figure 3. Comparison of linear viscoelastic τ_s of the slow process of various SI and styrene−butadiene (SB) micelles with two kinds of Stokes−Einstein diffusion time, $\tau_{SE,mat}$ and $\tau_{SE,cor}$. The copolymer code numbers indicate $10^{-3}M_S-10^{-3}M_{I/B}$. Parts a and b respectively show double-logarithmic plots of $\tau_{SE,mat}$ and $\tau_{SE,cor}$ against τ_s for dilute micelles, and parts c and d show the plots for concentrated micelles. Solid lines indicate relationships, $\tau_{SE,mat} = \tau_s$ (in parts a and c) and $\tau_{SE,cor} = \tau_s$ (in parts b and d). The data for SI blends in entangling and nonentangling hI matrices are shown with the large symbols with and without pips, respectively, and the data for SB blends in a nonentangling hB matrix[4] ($M = 2 \times 10^3$) are shown with the small filled symbols.

for $M_{matrix} > M_c$ with $M_c \cong 10^4$ for hI[19] (cf. Figure 2a). The M_{matrix} dependence of τ_{corona} (filled symbols in Figure 2b) is related to the corona dynamics in the following way: For $M_{matrix} < M_c$, the corona blocks exhibit their intrinsic relaxation behavior free from an effect of the corona−matrix entanglement and thus have M_{matrix}-insensitive τ_{corona} in the iso-ζ state. In contrast, for $M_{matrix} > M_c$, τ_{corona} increases with M_{matrix} because of a significant constraint release (CR) effect from the matrix, as fully discussed previously.[5] (For the pure CR mechanism, the corona relaxation is activated by the motion of the entangling matrix chains to have τ_{corona} essentially proportional to τ_{matrix}.)

In Figure 2b, we also note that τ_s (micelle diffusion time) and τ_{corona} of 15 wt % blends exhibit nearly the same M_{matrix} dependence while for the 5 wt % blends the dependence is stronger for τ_s than for τ_{corona}. This result suggests a difference in the diffusion behavior of the concentrated (15 wt %) and dilute (5 wt %) micelles. This difference can be examined by comparing the τ_s data with two kinds of Stokes−Einstein (SE) time utilizing the $\eta_{0,matrix}$ and $\eta_{0,corona}$ data as the effective viscosity for the micelle diffusion:[6]

$$\tau_{SE,mat} = \pi R_{micelle}\eta_{0,matrix}d_S^2/k_BT \qquad (2)$$

$$\tau_{SE,cor} = \pi R_{micelle}\eta_{0,corona}d_S^2/k_BT \qquad (3)$$

Here, k_B is the Boltzmann constant, T is the absolute temperature, d_S is the S core diameter (= diffusion distance for the slow process[7−9]), and $R_{micelle}$ is the micelle radius: $R_{micelle}$ is estimated to be $0.5d_S + 2^{1/2}R_{I,\theta}$, where $R_{I,\theta}$ is the unperturbed end-to-end distance of the I block and the factor $2^{1/2}$ accounts for expansion of the corona I blocks due to the steric repulsion[22] from the S core (having d_S comparable to $R_{I,\theta}$).[2,4] The d_S and $R_{I,\theta}$ values for our micelles, $d_S \cong 42$ nm and $R_{I,\theta} \cong 29$ nm for SI 68-122 and $d_S \cong 16$ nm and $R_{I,\theta} \cong 14$ nm for SI 14-29, were estimated from SAXS data of structurally similar micelles[23] and the unperturbed radius of gyration of hI chains.[24]

For the SI micelles examined in this study, Figure 3 shows plots of $\tau_{SE,mat}$ and $\tau_{SE,cor}$ against the τ_s data. The unfilled circles and square with pip indicate the plots for the SI 68-122 and SI 14-29 micelles in the entangling matrices (I-33 and I-19), and the unfilled circles without pip are for the SI 68-122 micelles in the nonentangling matrices (I-8 and I-2). The unfilled squares and triangle without pip show the plots for the previously examined SI micelles,[2] SI 14-29 and SI 43-86 ($M_S = 43.2 \times 10^3$, $M_I = 85.8 \times 10^3$) in a nonentangling I-4 matrix ($M = 4.1 \times 10^3 < M_e°$), and the small filled symbols are for

styrene−butadiene (SB) diblock copolymer micelles in a nonentangling B-2 matrix[4] ($M = 2 \times 10^3$). In all these systems, the matrix chains were considerably shorter than the corona blocks, and these blocks were in the wet brush state.[9]

In parts a and b of Figure 3, $\tau_{SE,mat}$ and $\tau_{SE,cor}$ of the dilute micelles (having no corona−corona entanglement) are double-logarithmically plotted against the τ_s data. As seen in part a, $\tau_{SE,mat}$ is in close agreement with τ_s. An agreement is found also between $\tau_{SE,cor}$ and τ_s (part b) because $\eta_{0,corona}$ of the dilute micelles examined were incidentally close to $\eta_{0,matrix}$. However, this incidental agreement vanishes on a further decrease of the micelle concentration: $\eta_{0,corona}$ of the dilute micelles is essentially proportional to the micelle concentration, and thus $\tau_{SE,cor}$ ($\propto \eta_{0,corona}$) vanishes at infinite dilution, while τ_s of those micelles becomes constant (>0) on infinite dilution. In part b, this behavior is most clearly noted for the dilute SI 14-29 micelles in the same matrix (I-4) but having different concentrations (= 8 and 15 wt %); see the unfilled squares connected with a dotted curve. These results demonstrate that the diffusion of the dilute micelles is governed by the matrix viscosity $\eta_{0,matrix}$.

In contrast, for the concentrated micelles having the corona−corona entanglement, $\tau_{SE,mat}$ is not correlated with τ_s and smaller than τ_s, while $\tau_{SE,cor}$ is close to τ_s (in particular for the SI micelles); see parts c and d of Figure 3. Thus, the diffusion of the concentrated micelles is governed by the corona viscosity $\eta_{0,corona}$. This result is naturally expected from a fact that the concentrated (mutually entangled) micelles are elastically coupled through their corona blocks, and their diffusion occurs only after these blocks relax.[3,6]

3.3. Overview of Nonlinear Relaxation Behavior. For the 15 and 5 wt % SI 68-122 blends in the entangling I-19 matrix, Figure 4 shows double-logarithmic plots of the nonlinear relaxation modulus $G(t,\gamma)$ at 25 °C against the time t. The $G(t,\gamma)$ data were measured at 5 and 25 °C, and the data at 5 °C were reduced at 25 °C with the aid of the shift factor for the linear viscoelastic G^* data. At these temperatures, the S cores were glassy (to have the modulus $\sim 10^9$ Pa) and hardly deformed by the stress due to the step strain, $\gamma G(t,\gamma)$. The thick and thin arrows indicate the relaxation times of the fast and slow processes of the SI 68-122 micelles in the linear viscoelastic regime, τ_{corona} and τ_s, and the solid curves denote the linear relaxation modulus $G(t)$ evaluated from the G^* data.

In Figure 4, the $G(t,\gamma)$ data exhibit two-step relaxation exclusively attributed to the fast and slow processes of the micelles. (The relaxation of the matrix was too fast to be detected in our experimental window.) $G(t,\gamma)$ agrees with $G(t)$ (solid curve), and the linear behavior prevails for small strains γ, while $G(t,\gamma)$ for large γ exhibits nonlinear damping (decrease) from $G(t)$. This damping is much stronger for the slow process than for the fast process. We also note that the damping of the slow process is more significant for the concentrated micelles (Figure 4a) than for the dilute micelles (Figure 4b). Similar behavior was observed for all SI blends in entangling/nonentangling matrices.

For dilute micelles in a nonenatngling matrix, the time-strain separability was found in the previous study.[17] The data in Figure 4 suggest the separability for the slow process of our concentrated/dilute SI 68-122 micelles in the entangling I-19 matrix. This separability is further tested in Figures 5 and 6 where the $G(t,\gamma)$ data of all concentrated and dilute SI 68-122/hI micelles are semilogarithmically plotted against the time t. The terminal tail characterized with the linear relationship between log $G(t,\gamma)$ and t is observed for all micelles at long t, and the terminal relaxation rate is insensitive to the strain γ; see dotted lines. This relaxation rate agreed well with the equilibrium relaxation frequency, $1/\tau_s$. Thus, the time-strain separability holds for the late stage of the slow process of either concentrated (15 wt %) or dilute (5 wt %) SI 68-122 micelles in both entangling and nonentangling matrices. The damping function $h_s(\gamma)$ of this process is evaluated as a vertical shift factor required for superimposing the terminal tails for large γ on the tail in the linear viscoelastic regime.

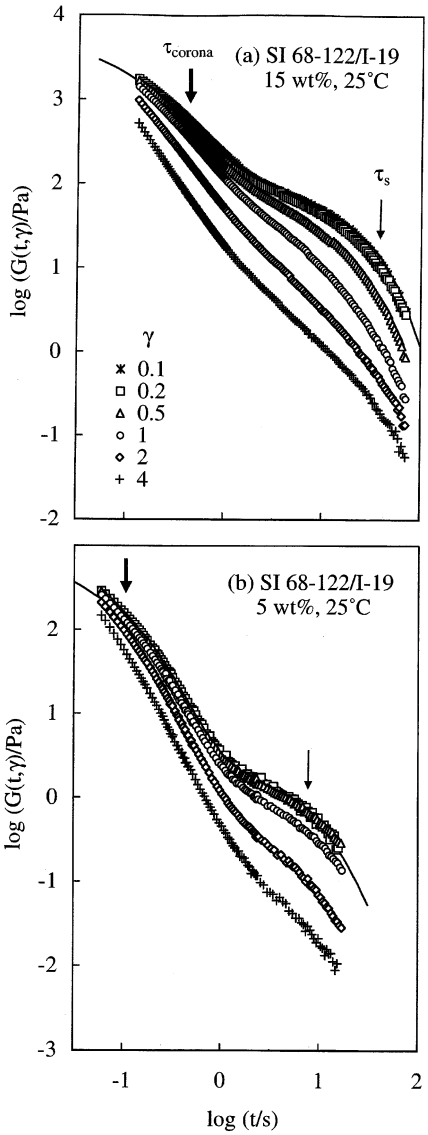

Figure 4. Double-logarithmic plots of nonlinear relaxation modulus $G(t,\gamma)$ of the 15 and 5 wt % SI 68-122/I-19 blends at 25 °C against time t. The data were measured at 5 ad 25 °C, and the data at 5 °C were reduced at 25 °C with the aid of the shift factor for linear viscoelastic G^* data. Solid curves indicate the linear relaxation modulus $G(t)$ evaluated from the G^* data.

For respective series of the SI 68-122 micelles having the same C_{SI} (= 15 and/or 5 wt %) in various matrices, parts a−d of Figures 5 and/or 6 demonstrate that the damping of the slow process becomes stronger with decreasing matrix molecular weight. Similar behavior

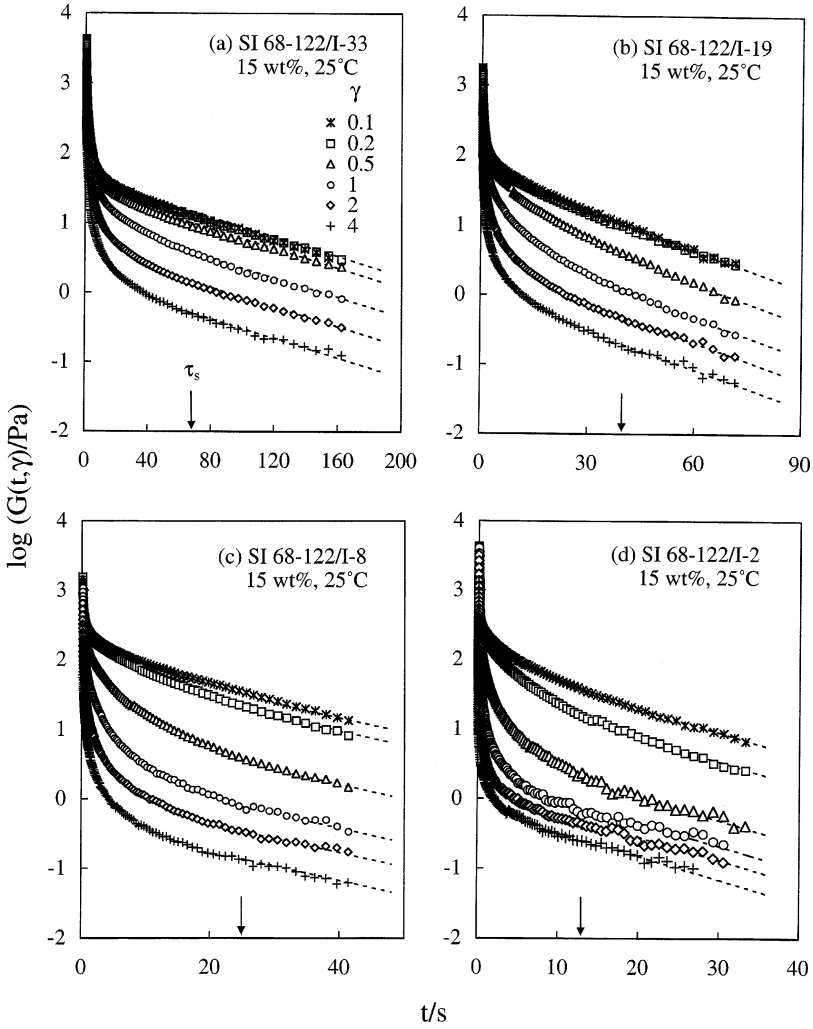

Figure 5. Semilogarithmic plots of nonlinear relaxation modulus $G(t,\gamma)$ of 15 wt % SI 68-122 blends in various hI matrices against time t. The data were measured at 5 and 25 °C, and the data at 5 °C were reduced at 25 °C with the aid of the shift factor for linear viscoelastic G^* data. Dotted lines indicate the terminal tails of the $G(t,\gamma)$ data.

was observed for the 15 wt % SI 14-29 micelles in the I-19 and I-4 matrices (the latter examined in the previous study[17]). Furthermore, the damping in each matrix is stronger for larger C_{SI}, as noted from comparison of Figures 5 and 6. These features of the slow process are later discussed in relation to the damping mechanism of this process.

3.4. Evaluation of Damping Functions. In the previous test of the nonlinear feature of the fast process (corona relaxation),[17] we subtracted the nonlinear relaxation modulus $G_s(t,\gamma)$ for the slow process from the raw $G(t,\gamma)$ data to evaluate the modulus for the fast process, $G_f(t,\gamma)$. We utilized this method to evaluate $G_f(t,\gamma)$ for our SI 68-122/hI and SI 14-29/I-19 blends, as explained below.

In this evaluation, we first focused on the raw $G(t,\gamma)$ data at long $t \geq 10\tau_{corona}$ with τ_{corona} being the corona relaxation time in the linear regime (cf. Figure 2b). In this range of t, the modulus due to the corona should fully relax and the raw data should coincide with $G_s(t,\gamma)$ for the slow process. Thus, the data at those t were fitted with a sum of exponential decay functions $G_{s,fit} = \sum_p g_{p,fit} \exp(-t/\tau_{p,fit})$, and this $G_{s,fit}$ was subtracted from the $G(t,\gamma)$ data at shorter t to evaluate $G_f(t,\gamma)$. Figure 7 shows typical results obtained for the 15 wt % SI 68-122/I-19 blend in the linear regime ($\gamma = 0.1$) and the highly nonlinear regime ($\gamma = 4$). The raw data (unfilled symbols) were well described by the fitted $G_{s,fit}$ (solid curves) at long t, and the subtraction successfully gave $G_f(t,\gamma)$ (small filled symbols). For all blends examined, $G_f(t,\gamma)$ were similarly obtained and $G_f(t,\gamma)$ for small γ (≤ 0.2) were independent of γ. In the following analysis, $G_f(t,\gamma)$ for $\gamma \leq 0.2$ is utilized as the linear relaxation modulus $G_f(t)$ for the fast process.

As noted in Figure 7, the nonlinear $G_f(t,\gamma)$ data (for $\gamma = 4$) and linear $G_f(t)$ data (for $\gamma = 0.1$) exhibit nearly the same t dependence at long t, suggesting the validity of the time-strain separability $G_f(t,\gamma) = h_f(\gamma)G_f(t)$ at long t. Indeed, this separability was found for all SI/hI blends. As an example, Figure 8 shows the $G_f(t,\gamma)$ data of the 15 and 5 wt % SI 68-122/I-19 blends normalized by respective damping functions $h_f(\gamma)$. These data are excellently superimposed on the linear $G_f(t)$ data ($= [G_f(t,\gamma)]_{\gamma \leq 0.2}$), and the separability is confirmed.

Thus, for the concentrated/dilute micelles in either entangling or nonentangling micelles, the time-strain separability holds for both of the fast and slow processes, and $G(t,\gamma)$ can be expressed as

$$G(t,\gamma) \cong h_f(\gamma)\, G_f(t) + h_s(\gamma)\, G_s(t) \qquad (4)$$

The linear relaxation modulus and damping function for the fast process, $G_f(t)$ and $h_f(\gamma)$, are evaluated with the methods explained for Figures 7 and 8. The linear

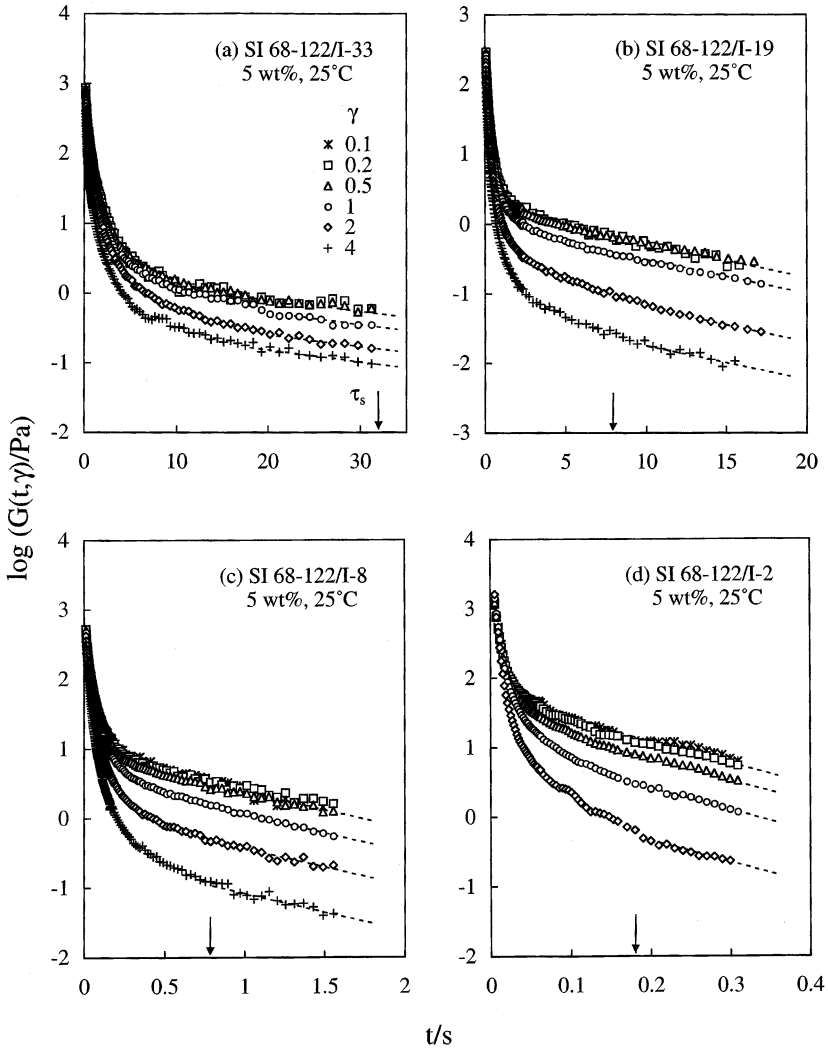

Figure 6. Semilogarithmic plots of nonlinear relaxation modulus $G(t,\gamma)$ of 5 wt % SI 68-122 blends in various hI matrices against time t. The data were measured at 5 ad 25 °C, and the data at 5 °C were reduced at 25 °C with the aid of the shift factor for linear viscoelastic G^* data. Dotted lines indicate the terminal tails of the $G(t,\gamma)$ data.

modulus for the slow process, $G_s(t)$, is evaluated as the function $G_{s,fit} = \sum_p g_{p,fit} \exp(-t/\tau_{p,fit})$ that fits the linear $G(t)$ data of the blends at long t ($\geq 10\tau_{corona}$), and the damping function $h_s(\gamma)$ for this process is simply evaluated as the vertical shift factor required for the superposition of the terminal tails of the $G(t,\gamma)$ data having the γ-insensitive τ_s (cf. Figures 5 and 6). The non-Newtonian behavior of the micellar blends under fast flow was well correlated with the damping behavior under large strains (eq 4) through a BKZ constitutive equation, as explained in the Appendix.

Focusing on the $h_f(\gamma)$ and $h_s(\gamma)$ data thus obtained, we examined the damping mechanisms for the SI micelles in the entangling/nonentangling matrices. The results are summarized below, first for the fast process detecting the corona relaxation and then for the slow process reflecting the micelle diffusion.

3.5. Damping Mechanism for Fast Process. For all SI micelles examined, the fast process satisfies the time-strain separability. In Figure 9, the $h_f(\gamma)$ data for this process (large symbols) are compared with the $h(\gamma)$ data for entangled linear/star homopolymers[25,26] (small circles) and nonentangled linear homopolymers[27] (small squares).

For the entangled homopolymers, $h(\gamma)$ is universally dependent on γ irrespective of their molecular weight.[28−30] This behavior is attributed to the retraction of the strain-elongated chains that occurs before the global rotational motion (orientational relaxation) of the chain, and the universal γ dependence is close to the tube model prediction.[29,30] The time-strain separable damping observed for the nonentangled chains[27] indicates that a similar mechanism (retraction faster than rotation) works also for these chains, although the damping is weaker for the nonentangled chains than for the entangled chains, and the details of this mechanism for the nonentangled chains have not been clarified yet.

As seen in Figure 9, the $h_f(\gamma)$ data of the SI micelles are close to the $h(\gamma)$ data of the homopolymers. This fact strongly suggests that the damping of the fast process of the micelles is similar to that of the homopolymers and thus related to the retraction of the strain-elongated corona blocks occurring in prior to the orientational relaxation of the corona. A detailed inspection indicates that the $h_f(\gamma)$ data of the mutually entangled and nonentangled corona blocks respectively are close to but a little smaller than $h(\gamma)$ of the entangled and nonentangled homopolymers. This difference may be partly related to the filler effect from the rigid S cores (that enlarge the local strain and enhance the damping). However, this difference is rather minor, and the

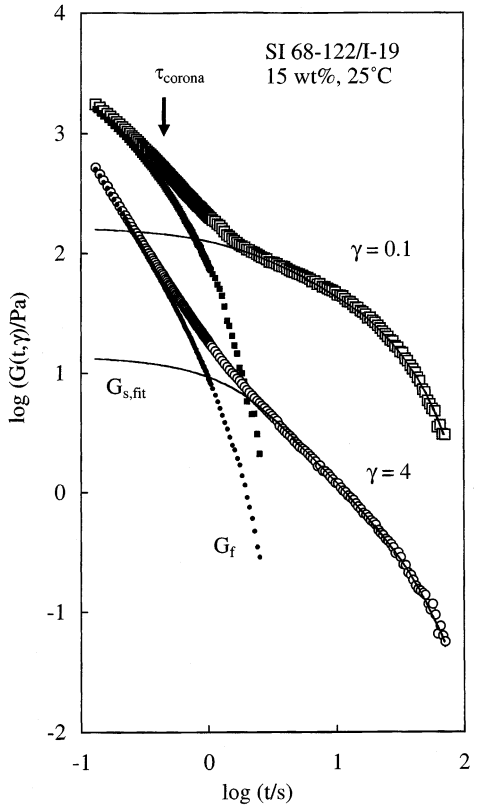

Figure 7. Separation of the $G(t,\gamma)$ data of the 15 wt % SI 68-122/I-19 blend into the moduli $G_f(t,\gamma)$ and $G_s(t,\gamma)$ for the fast and slow relaxation processes. The results are shown for $\gamma = 0.1$ (in the linear regime) and $\gamma = 4$ (in the nonlinear regime).

nonlinear damping of the fast process of the SI micelles is essentially attributable to the retraction of the strain-elongated corona blocks.

3.6. Damping Mechanism for Slow Process. For the concentrated/dilute SI micelles in either entangling or nonentangling matrices, the slow process (micelle diffusion process) exhibits the time-strain separable damping. For the concentrated and dilute micelles, the $h_s(\gamma)$ data of the slow process are shown in Figure 10a,b. For comparison, Figure 10a also shows the $h(\gamma)$ data for the Brownian suspensions of silica particles (of radius = 40 nm) in ethylene glycol/glycerol mixture containing salt (KCl);[15,16] cf. small filled symbols. The effective volume fraction ϕ_{eff} of these particles, representing the bare volume fraction plus a contribution from a short-ranged interparticle electrostatic repulsion not fully screened by the salt, ranges from 0.36 to 0.59.

For the silica suspensions, $h(\gamma)$ decreases with increasing ϕ_{eff} (see Figure 10a). Similarly, $h_s(\gamma)$ of the SI micelles in a given (either entangling or nonentangling) matrix decreases with the micelle concentration C_{SI} (cf. Figures 4−6 and 10). Furthermore, $h_s(\gamma)$ of the micelles are close, in magnitude and γ dependence, to $h(\gamma)$ of the silica suspensions (see Figure 10a). These similarities between the SI micelles and silica suspensions provide us with a clue for examining the entanglement effects on the nonlinearity of the SI micelles, as discussed below.

For the silica suspensions, $G(t,\gamma)$ detects the nonlinear relaxation of the Brownian stress σ_B. This σ_B reflects the anisotropy of the spatial distribution of the particles, and the damping is attributed to the γ-insensitivity of this anisotropy for large γ.[15,16] At large ϕ_{eff}, the particles

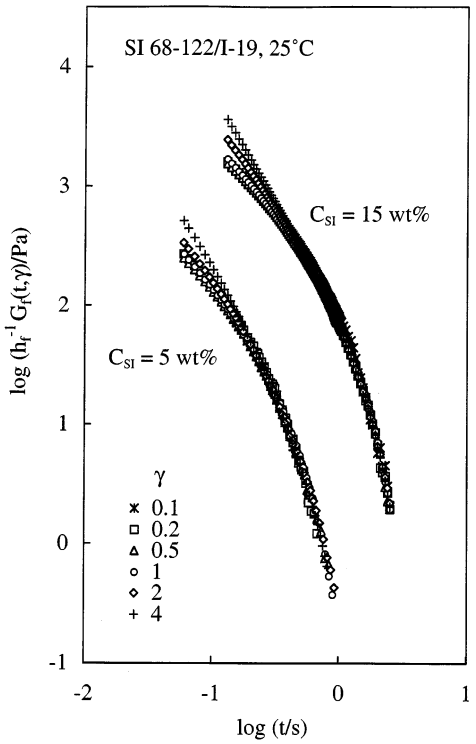

Figure 8. Comparison of the normalized relaxation moduli $h_f^{-1}G_f(t,\gamma)$ ($\gamma = 0.1-4$) for the fast process of the 15 and 5 wt % SI 68-122/I-19 blends.

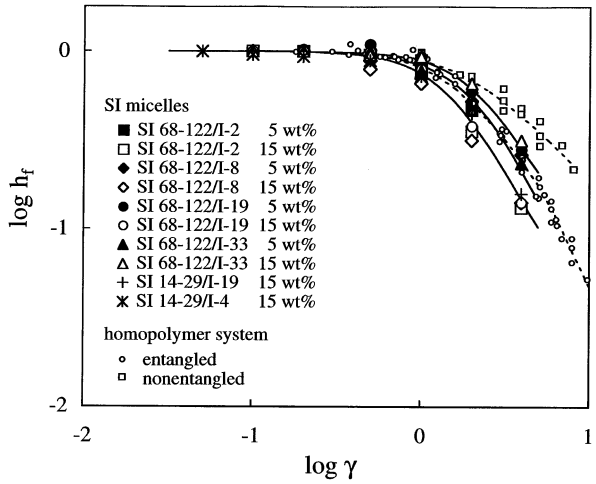

Figure 9. Damping function $h_f(\gamma)$ for the fast process of the SI/hI blends as indicated (large symbols). For comparison, $h(\gamma)$ data are also shown for entangled linear/star homopolstyrene solutions[25,26] (small circles) and nonentangled linear homopolystyrene solutions[27] (small squares).

significantly collide with each other on imposition of a large step strain to exhibit relative, rotational motion. This motion occurs nonaffinely and is similar to random mixing. Thus, the distribution anisotropy is reduced by the particle collision/relative rotation, resulting in the enhancement of the damping for larger ϕ_{eff}.[16]

Similarity, the nonlinear damping of the slow process of the micelles can be attributed to the γ-insensitivity of the micelle distribution anisotropy under large strains, and the decrease of $h_s(\gamma)$ in a given matrix with increasing C_{SI} can be related to the strain-induced collision/relative rotation of the micelles enhanced for larger C_{SI}.

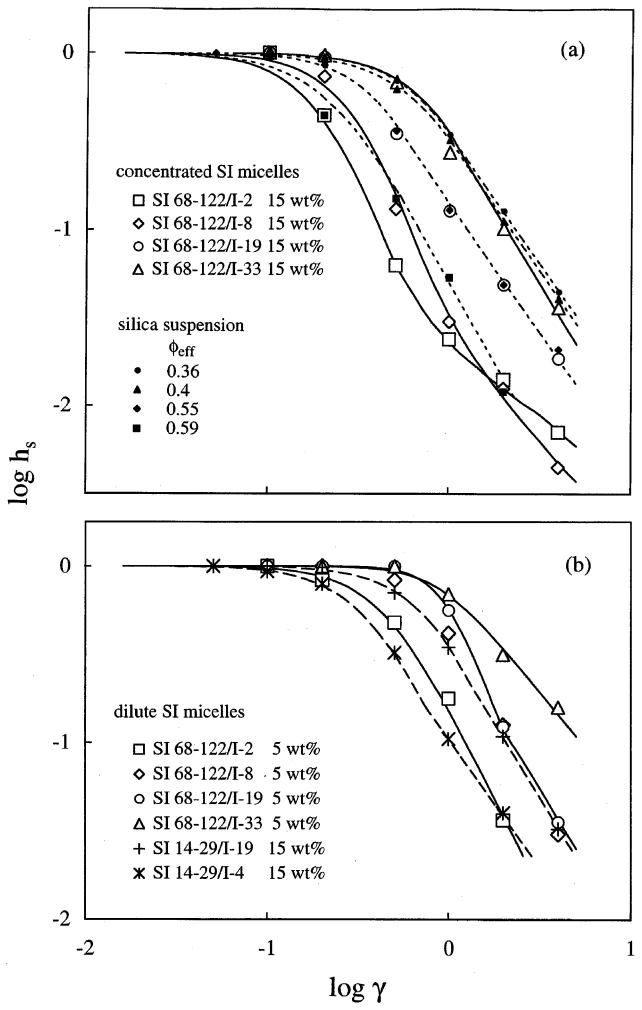

Figure 10. Damping function $h_s(\gamma)$ for the slow process of (a) concentrated SI/hI blends and (b) dilute SI/hI blends as indicated (large symbols). For comparison, $h(\gamma)$ of Brownian suspensions of silica particles[15,16] having effective volume fractions $\phi_{eff} = 0.36-0.59$ are shown in part a (small filled symbols).

For respective series of the SI 68-122 and/or SI 14-29 micelles having the same C_{SI} in various matrices, $h_s(\gamma)$ increases and the nonlinearity is reduced with increasing matrix molecular weight M_{matrix}, as clearly noted in Figure 10a,b. This behavior can be related to the above damping mechanism: The strain-induced collision/relative rotation of the micelles should raise an extra strain in the matrix, and the matrix elasticity would tend to diminish this strain, thereby disturbing the rotation and reducing the nonlinearity. This elastic effect should be enhanced in the high-M matrices forming long-lived corona−matrix entanglements, and the reduction of the nonlinearity with increasing M_{matrix} is attributed to that effect.

In relation to this molecular picture, one may expect that the corona−corona entanglement of the SI 68-122 micelles formed on the increase of C_{SI} (from 5 to 15 wt %) also tends to disturb the relative rotation of the colliding micelles and reduce the nonlinearity. This disturbance counteracts an enhancement of the strain-induced collision/rotation of micelles intrinsically occurring on the increase of C_{SI} (collision probability $\sim C_{SI}^2$). Since the relaxation of the corona−corona entanglement becomes slower with increasing M_{matrix} (due to the constraint release effect from the matrix; cf. Figure 2b), the disturbance for the rotation due to this entanglement would be more important and thus the decrease of $h_s(\gamma)$ on the increase of C_{SI} would be less significant for larger M_{matrix}. This argument is in harmony with the experimental observation.

3.7. Additional Comment for the Time-Strain Separability of the Slow Process. The time-strain separability holds for the micelle diffusion process (slow process) because the terminal relaxation time of this process, τ_s, does not change with the strain γ. Since τ_s for the concentrated and dilute micelles are governed by the corona and matrix viscosities (cf. Figure 3), the separability means that these viscosities are independent of γ in a time scale of micelle diffusion. This argument may sound trivial because the micelle diffusion is much slower than the corona/matrix relaxation (cf. Figure 2b) and the corona blocks/matrix chains should exhibit their linear viscoelastic (equilibrium) behavior in that time scale. However, a comment needs to be added for the early stage of the micelle diffusion in relation to the experimental results reported by Isono and co-workers[31−35] and Archer and co-workers.[36,37]

Isono and co-workers examined the entanglement density of high-M polyisobutylene and poly(vinyl ethylene) under large step strains by superimposing a small-amplitude oscillation thereon. They found that a viscoelastic modulus defined for this oscillation (of the frequency at the middle of the rubbery plateau zone) is smaller than the linear viscoelastic modulus and concluded a decrease of the entanglement density due to large step strains.[38] This decrease was also noted by Archer and co-workers[37] from analysis of the nonlinear relaxation modulus data of high-M polystyrene solutions. Archer[36] also examined the nonlinear behavior under fast flow by superimposing a small step strain thereon and found a flow-induced decrease of the entanglement density.

Under step strains, the entanglement density gradually recovers its equilibrium value with time, but this recovery is slower than the stress relaxation[31−35] (as most clearly observed in Figure 3 of ref 34). This result is conceivable if we consider a fact that the stress reflects both of the orientational anisotropy and entanglement density of the chain[31−37] and the stress relaxes whenever the anisotropy vanishes *even before* the complete recovery of the equilibrium entanglement density. (This recovery appears to require a mutual displacement of the chains over a considerably large length scale, as judged from the results by Isono and co-workers.) In relation to this point, Archer and co-workers[37] suggested that the recovery (reentanglement) occurs on a time scale of constraint release (CR): For high-M linear chains, the CR time is considerably longer than the measured stress relaxation time.[29]

This behavior of homopolymers suggests that the entangled corona blocks and matrix chains in our SI/hI blends would recover their linear viscoelastic viscosity and the equilibrium entanglement density in a time scale longer than respective relaxation times. However, for the matrix chains having the relaxation time τ_{matrix} much shorter than τ_s for the micelle diffusion ($\tau_{matrix} < 10^{-4}\tau_s$; cf. Figure 1), a strain-induced nonlinear decrease of their viscosity would vanish at $t \ll \tau_s$, and even the early stage of micelle diffusion would be negligibly affected by this decrease. In contrast, the mutually entangled corona blocks of the concentrated micelles have $\tau_{corona} \cong 10^{-2}\tau_s$ (cf. Figure 2b), and the nonlinear

decrease of their viscosity may remain in the early stage of the micelle diffusion (but not in the late stage detected as the terminal relaxation of the SI/hI blends). For this case, the early stage diffusion of the concentrated micelles is expected to be accelerated under large strains. It is an interesting subject of future work to test this expectation (through a diffusion measurement for dye-labeled micelles under large strains, for example).

4. Concluding Remarks

We have examined nonlinear relaxation behavior of SI micelles randomly dispersed in homopolyisoprene matrices. These micelles exhibited fast and slow relaxation processes in the linear viscoelastic regime, the former representing the orientational relaxation of individual corona I blocks tethered on glassy S cores and the latter detecting the relaxation of the Brownian stress σ_B. This σ_B reflects the anisotropy of the micelle distribution and its relaxation is induced by the micelle diffusion (over a distance $\cong$ S core diameter). Under large step strains, the time-strain separable nonlinear damping was observed for both of the fast and slow processes, and the damping was much stronger for the slow process. The thinning corresponding to this damping was observed under fast shear.

For the concentrated/dilute micelles with/without the corona−corona entanglement, the damping function for the fast process $h_f(\gamma)$ was close to $h(\gamma)$ of homopolymers. This result, commonly observed in either entangling or nonentangling matrices, indicates that the damping of the fast process is essentially attributed to retraction of the strain-elongated corona blocks occurring in prior to their rotational motion (orientational relaxation), as similar to the situation for homopolymers.

The damping function for the slow process $h_s(\gamma)$ was close to $h(\gamma)$ of Brownian suspensions of silica particles, suggesting that the damping of this process reflects the strain insensitivity of the anisotropy of the micelle distribution for large γ. Furthermore, for the concentrated/dilute micelles, the damping was weaker in the entangling matrix than in the nonentangling matrix. This result suggests that the corona−matrix entanglement elastically disturbs the relative rotation of the micelles on the strain-activated intermicellar collision. (This rotation is similar to random mixing so that the disturbance for the rotation reduces the nonlinearity and weakens the damping.) The corona−corona entanglement gives a similar elastic effect on the damping behavior.

Appendix. Non-Newtonian Behavior under Fast Flow

Our previous studies showed that the dilute SI 14-29 micelles in the nonentangling I-4 matrix exhibit the time-strain separable damping under large strains[17] ($G(t,\gamma) \cong h_f(\gamma)G_f(t) + h_s(\gamma)G_s(t)$; eq 4), and their non-Newtonian flow behavior can be well correlated with this damping behavior through a BKZ constitutive equation incorporating eq 4.[18] In this study, we confirmed the time-strain separability for the concentrated/dilute SI micelles in both entangling and nonentangling matrices (cf. Figures 4−6 and 8). For completeness of rheological characterization, we conducted the steady flow measurements for the SI 68-122 and SI 14-29 micelles in the entangling I-19 matrix and compared the viscosity data with the BKZ calculation. The results are summarized below.

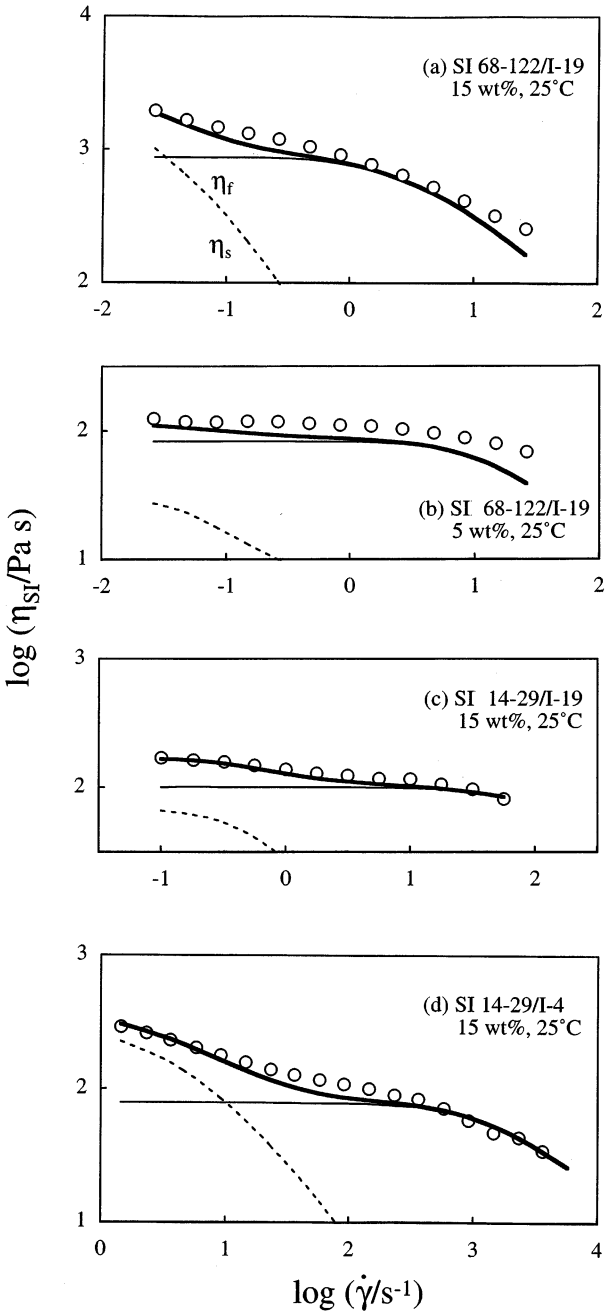

Figure 11. Steady-state viscosity η_{SI} at 25 °C obtained for various SI micelles as indicated (circles). The thick solid curves denote η_{SI} calculated from a BKZ constitutive equation utilizing the nonlinear damping data, and the thin solid and dotted curves indicate the viscosities $\eta_f(\dot{\gamma})$ and $\eta_s(\dot{\gamma})$ calculated for the fast and slow processes, respectively. For further details, see the Appendix.

Combining the BKZ equation with eq 4, we can calculate the steady-state viscosity $\eta(\dot{\gamma})$ of the micellar blends at a shear rate $\dot{\gamma}$ as[18]

$$\eta(\dot{\gamma}) = \phi_{matrix}\eta_{0,matrix} + \eta_f(\dot{\gamma}) + \eta_s(\dot{\gamma}) \qquad (A1)$$

with

$$\eta_x(\dot{\gamma}) = -\int_0^\infty \frac{dG_x(t)}{dt} h_x(\gamma_t)t\, dt \quad (x = f, s) \qquad (A2)$$

Here, ϕ_{matrix} is the volume fraction of the matrix in the blend, $\gamma_t (= \dot{\gamma} \times t)$ is the strain at time t imposed through

the flow, and $G_x(t)$ and $h_x(\gamma)$ are the linear relaxation moduli and nonlinear damping functions for the fast and slow processes (x = f and s). (Equation A1 assumes the Newtonian behavior of the matrix at the shear rates examined, which was consistent with experiments for the pure matrix.) The viscosity due only to the micelles is given by $\eta_{SI}(\dot{\gamma}) = \eta_f(\dot{\gamma}) + \eta_s(\dot{\gamma})$.

For the concentrated SI 68-122 micelles and dilute SI 68-122/SI 14-29 micelles in the entangling I-19 matrix, parts a−c of Figure 11 compare the BKZ calculation with the $\eta_{SI}(\dot{\gamma})$ data (obtained by subtracting the matrix contribution $\phi_{matrix}\eta_{0,matrix}$ from the $\eta(\dot{\gamma})$ data). The comparison is also made for the previously examined dilute SI 14-29 micelles in the nonentangling I-4 matrix[18] (part d). For all cases, the BKZ calculation (thick solid curves) is close to the data (circles), confirming that the thinning behavior of the concentrated/dilute micelles in both entangling and nonentangling matrices is well correlated to the damping behavior. Although not shown here, the BKZ calculation also described the time-dependent (transient) growth of the stress after start-up of flow. These results strongly suggest that the thinning has the same molecular origin as the damping. Thus, for the concentrated/dilute micelles in either entangling or nonentangling matrices, the thinning is attributable to the $\dot{\gamma}$-insensitive micelle distribution occurring at small $\dot{\gamma}$ (cf. $\eta_{s,BKZ}$ shown with the thin dotted curves in Figure 11) and the flow-induced distortion of the corona block conformation occurring at large $\dot{\gamma}$ (cf. $\eta_{f,BKZ}$ shown with the thin solid curves).

Here, a comment needs to be added for the BKZ calculation. Equation 4 assumes the t-independent $G_f(t,\gamma)/G_f(t)$ and $G_s(t,\gamma)/G_s(t)$ ratios in the entire range of t. However, these ratios actually decay with t and converge to the t-independent damping functions $h_f(\gamma)$ and $h_s(\gamma)$ only in respective terminal regimes of the fast and slow processes (cf. Figures 5, 6, and 8). Thus, eq 4 incorporated in our simple BKZ calculation is approximate. Nevertheless, the viscosity is dominated by $G_f(t,\gamma)$ and $G_s(t,\gamma)$ in respective terminal regimes. This allowed the simple BKZ calculation to satisfactorily describe the data.

References and Notes

(1) Watanabe, H.; Kotaka, T. *J. Rheol.* **1983**, *27*, 223.
(2) Sato, T.; Watanabe, H.; Osaki, K.; Yao, M. L. *Macromolecules* **1996**, *29*, 3881.
(3) Watanabe, H. *Acta Polym.* **1997**, *48*, 215.
(4) Watanabe, H.; Sato, T.; Osaki, H. *Macromolecules* **1996**, *29*, 104.
(5) Watanabe, H.; Sato, T.; Osaki, H. *Macromolecules* **1996**, *29*, 113.
(6) Watanabe, H. *Kobunshi Ronbunshu* **2001**, *58*, 135.
(7) Watanabe, H.; Sato, T.; Osaki, K.; Hamersky, M. W.; Chapman, B. R.; Lodge, T. P. *Macromolecules* **1998**, *31*, 3740.
(8) Gohr, K.; Pakula, T.; Tsutsumi, K.; Schartl, W. *Macromolecules* **1999**, *32*, 7156.
(9) Gohr, K.; Schartl, W. *Macromolecules* **2000**, *33*, 2129.
(10) van der Werff, J. C.; de Kruif, C. G.; Blom, C.; Mellema, J. *Phys. Rev. A* **1989**, *39*, 795.
(11) Mellema, J.; van der Werff, J. C.; Blom, C. de Kruif, C. G. *Phys. Rev. A* **1989**, *39*, 3696.
(12) Shikata, T.; Pearson, D. S. *J. Rheol.* **1994**, *38*, 601.
(13) Brady, J. F. *J. Chem. Phys.* **1993**, *99*, 567.
(14) Bender, J. W.; Wagner, N. J. *J. Colloid Interface Sci.* **1995**, *172*, 171.
(15) Watanabe, H.; Yao, M. L.; Yamagishi, A.; Osaki, K.; Shikata, T.; Niwa, H.; Morishima, Y. *Rheol. Acta* **1996**, *35,* 433.
(16) Watanabe, H.; Yao, M. L.; Osaki, K.; Shikata, T.; Niwa, H.; Morishima, Y. *Rheol. Acta* **1999**, *38*, 2.
(17) Watanabe, H.; Sato, T.; Osaki, K.; Yao, M. L. *Macromolecules* **1996**, *29*, 3890.
(18) Watanabe, H.; Yao, M. L.; Sato, T.; Osaki, K. *Macromolecules* **1997**, *30*, 5905.
(19) Ferry, J. D. *Viscoelastic Properties of Polymers*, 3rd ed.; Wiley: New York, 1980.
(20) Raju, V. R.; Menezes, E. V.; Marin, G.; Graessley. W. W.; Fetters, L. J. *Macromolecules* **1981**, *14*, 1668.
(21) Fetters, L. J.; Kiss, A. D.; Pearson, D. S.; Quack, G. F.; Vitus, F. J. *Macromolecules* **1993**, *26*, 647.
(22) Dimarzio, E. A. *J. Chem. Phys.* **1965**, *42*, 2101.
(23) Watanabe, H.; Kotaka, T. *Polym. J.* **1982**, *14*, 739.
(24) Tsunashima, Y.; Hirata, N.; Nemoto, N.; Kurata, M. *Macromolecules* **1988**, *21*, 1107.
(25) Osaki, K.; Nishizawa, K.; Kurata, M. *Macromolecules* **1982**, *15*, 1068.
(26) Osaki, K.; Takatori, E.; Kurata, M.; Watanabe, H.; Yoshida, H.; Kotaka, T. *Macromolecules* **1990**, *23*, 4392.
(27) Takatori, E.; Osaki, K.; Kurata, M.; Hirayama, T. *Nihon Reoroji Gakkaishi (J. Soc. Rheol. Jpn.)* **1988**, *16*, 99.
(28) (a) Osaki, K. *Rheol. Acta* **1993**, *32*, 429. (b) The universality of the damping function was reported to vanish for high-M monodisperse linear polymers (with $M > 50M_e$)[28a] possibly because of the instability discussed by Marrucci and Grizzuti.[28c] However, the mutually entangled corona blocks in our 15 wt % SI 68-122/hI blends have $M \cong 3M_e$ ($= 3M_e°/\phi_{corona}$), and this instability is negligible for these blocks. (c) Marrucci, G.; Grizzuti, N. *J. Rheol.* **1983**, *27*, 433.
(29) Watanabe, H. *Prog. Polym. Sci.* **1999**, *24*, 1253.
(30) Doi. M.; Edwards, S. F. *The Theory of Polymer Dynamics*; Clarendon: Oxford, UK, 1986.
(31) Isono, Y.; Itoh, K.; Komiyatani, T.; Fujimoto, T. *Macromolecules* **1991**, *24*, 4429.
(32) Isono, Y.; Shizuru, K.; Fujimoto, T. *Macromolecules* **1991**, *24*, 4433.
(33) Isono, Y.; Ohashi, N.; Kase, T. *Macromolecules* **1995**, *28*, 5154.
(34) Isono, Y.; Kamohara, T.; Takano, A.; Kase, T. *Rheol. Acta* **1997**, *36*, 245.
(35) Isono, Y.; Kawahara, S.; Kase, T. *Nihon Reoroji Gakkaishi (J. Soc. Rheol. Jpn.)* **2003**, *31*, 201.
(36) Archer, L. A. *J. Rheol.* **1999**, *43*, 1617.
(37) Archer, L. A.; Sanchez-Reyes, J.; Juliani *Macromolecules* **2002**, *35*, 10216.
(38) The entanglement density under large strains/fast flow can be quantitatively evaluated only after the viscoelastic responses against the superimposed oscillation/strain[31−36] are analyzed with the aid of an appropriate constitutive equation (because these responses would contain contributions from the large strain/fast flow). However, the decrease of the entanglement density under large strains/fast flow and its slow recovery to the equilibrium level can be qualitatively concluded from the raw data reported by Isono and coworkers[31−35] and by Archer[36] even without this analysis.

MA048544Z